Phys. Med. Biol. **42** (1997) 433–439. Printed in the UK PII: S0031-9155(97)75575-1

Validation of the central-ray approximation for attenuated depth-dependent convolution in quantitative SPECT reconstruction

Zhengrong Liang, Juihsi Cheng and Jinghan Ye

Departments of Radiology, Electrical Engineering and Computer Science, State University of New York, Stony Brook, NY 11794, USA

Received 3 June 1996, in final form 20 August 1996

Abstract. In order to model photon attenuation and detector resolution variation as a depth-dependent convolution for efficient reconstruction of quantitative SPECT, a central-ray approximation is necessary. This work investigates the impact of the approximation upon reconstruction accuracy and computational efficiency. A patient chest CT image was acquired and converted into an object-specific attenuation map. From a segmentation of the map, an emission thorax phantom was constructed with a cardiac insert. To generate a system-specific resolution-variant kernel, a point source was measured at several depths from the surface of a low-energy, high-resolution, parallel-hole collimator of a SPECT system. Projections of parallel-beam geometry were simulated from the phantom, the map, and the kernel on an elliptical orbit. Reconstruction was performed by the ML-EM algorithm with and without the central-ray approximation. The approximation cuts down dramatically (more than 100 fold) the computing time with a negligible loss (less than 1%) of reconstruction accuracy.

1. Introduction

Compensation for photon attenuation and detector resolution variation is a major component in reconstruction of quantitative SPECT (single-photon emission computed tomography) (Jaszczak 1988). While photon transportation within an attenuating body and photon detection by a collimator/detector SPECT system can be modelled by a projection equation (Liang 1992), inversion of the equation is very difficult (Riauka and Gortel 1994). Some assumptions and approximations are necessary for the inversion in order to implement quantitative SPECT for clinical use.

A central-ray approximation has been implicitly assumed when analytical inversion of the projection equation was attempted for uniform attenuating media and depth-dependent detector response (Appledorn 1989, van Elmbt and Walrand 1993). We have applied the approximation for iterative inversion of the projection equation in the cases of non-uniform attenuating media (for example the chest) and variable detector response (Liang *et al* 1988, 1989). A very simple ray-tracing model was used to study the approximation. The model assumed a zero contribution to a detection bin if the centre of a voxel is out of the view of that bin, and otherwise a whole-voxel contribution to that bin. Although the central-ray approximation seems reasonable (less than 1% error by the simple model), it has been argued for a while whether the approximation has a significant impact on the reconstruction accuracy for a more realistic ray-tracing model. This work aims to use an accurate ray-tracing model for both the object-specific attenuation and the system-specific detector response to investigate the approximation on the reconstruction accuracy.

0031-9155/97/020433+07$19.50

2. Theory

The projection equation for SPECT with parallel-beam collimation is given, if scatter contribution is neglected, (see figure 1), by (Liang 1992)

$$p(\xi, z, \theta) = \int_{-\infty}^{\infty} \mathrm{d}\eta \iint_{-\infty}^{\infty} \mathrm{d}\xi' \, \mathrm{d}z' \, h(\xi - \xi', z - z', \eta) o(\xi', z', \eta, \theta) \times \exp\left(- \int_{-\infty}^{\eta} \mu(\xi', z', \eta', \theta) \, \mathrm{d}\zeta \right) \tag{1}$$

where $o(\xi, z, \eta, \theta)$, $\mu(\xi, z, \eta, \theta)$ and $h(\xi, z, \eta)$ represent the source distribution $o(x, y, z)$, the attenuation map $\mu(x, y, z)$ and the detector-response kernel in the rotation coordinates (ξ-η-z), and $p(\xi, z, \theta)$ is the measurement at detection bin (ξ, z, θ) by projection angle θ. The integral for the attenuation factors is along line ζ, which covers both the central and off-centre rays within the resolution kernel (see figure 1). The collected counts at bin (ξ, z, θ) are the contributions from those voxels covered by the resolution kernel (or inside the view of the bin). At a fixed depth η, since the kernel $h(\xi, z, \eta)$ is shift invariant on the ξ–z plane, the contribution $o(\xi', z', \eta, \theta)$ of the voxel at (ξ', z', η) is weighted by $h(\xi - \xi', z - z', \eta)$ and is attenuated by a factor, which is computed by the integral along line ζ from bin (ξ, z, θ) to the voxel through the attenuation map. The attenuation factor is a function of $(\xi, \xi', z, z', \eta, \theta)$.

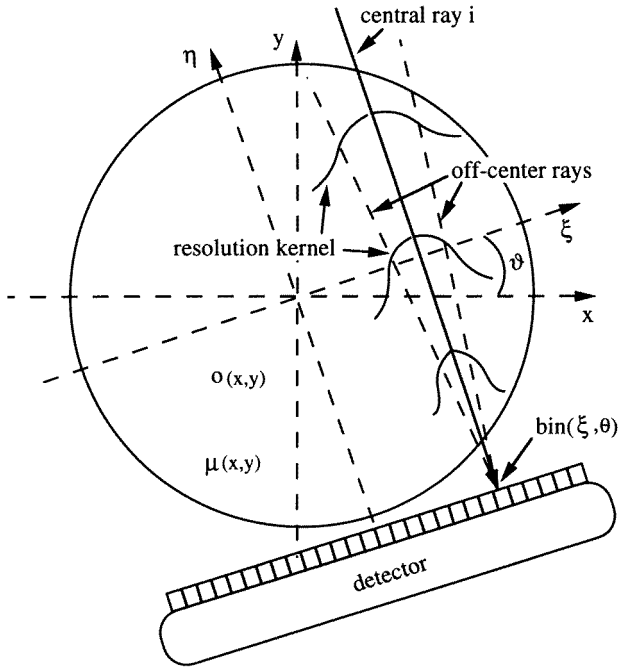

Figure 1. Two-dimensional geometric representation of photon detection in SPECT. The central rays are parallel to the collimator holes. The off-centre rays define the view of a detection bin, which depends on the size of the collimator holes and the intrinsic resolution of the detector crystal.

It can be seen that the computation for the attenuation factors by tracing all the rays from bin (ξ, z, θ) to those voxels (ξ', z', η) within the view of that bin is extremely intensive. A

readily available solution is to approximate those attenuation factors by that of the central ray i (see figure 1). With this central-ray approximation, equation (1) becomes

$$p(\xi, z, \theta) = \int_{-\infty}^{\infty} \mathrm{d}\eta \iint_{-\infty}^{\infty} \mathrm{d}\xi' \, \mathrm{d}z' \, h(\xi - \xi', z - z', \eta) \times \left[o(\xi', z', \eta, \theta) \exp\left(- \int_{-\infty}^{\eta} \mu(\xi', z', \eta', \theta) \, \mathrm{d}\eta' \right) \right] \tag{2}$$

where the integral for the attenuation factors is now parallel to the η-axis. At each projection angle θ, the attenuated source $o(\xi', z', \eta, \theta) \exp(- \int_{-\infty}^{\eta} \mu(\xi', z', \eta', \theta) \, \mathrm{d}\eta')$ can be calculated for each voxel. Then the double integral ($\mathrm{d}\xi' \mathrm{d}z'$) on the ξ-z plane at a constant depth η is a convolution of the attenuated source with the resolution kernel. Efficient inversion of equation (2) for $o(x, y, z)$ can be performed either analytically if activity is inside a uniform attenuating medium (Glick *et al* 1993, Liang *et al* 1994) or iteratively if activity is within a non-uniform attenuating body (Ye *et al* 1994, Zeng and Gullberg 1992).

Since the depth-dependent convolution of equation (2) is based on the central-ray approximation, validation of the approximation is necessary if the inversion of equation (2) is to be recommended for clinical use.

3. Method

In order to evaluate the impact of the central-ray approximation upon the accuracy of the reconstruction, the true source should be known. Phantom studies are customarily performed for this kind of evaluation. A validation based on phantom studies was, therefore, performed in both two-dimensional (2D) and 3D cases, as described below.

A patient chest image was acquired by a GE high-speed CT (computed tomography) scanner with a conventional protocol of 120 kVp and 280 mA. The image matrix was 512^2 on a field-of-view (FOV) of 48 cm diameter, a total of 64 slices with a thickness of 4 mm. The CT image was first converted into an attenuation-coefficient map for 140 keV photon energy (simulating a ^{99m}Tc labelled sestamibi myocardial perfusion study). Then the map was resized to $128^2 \times 64$ on a FOV of 51.2 cm (for a conventional large-field whole-body SPECT detector system). The voxel size was 4 mm with 4 mm thickness. The attenuation coefficient was approximately 0.06/voxel for the soft tissues which corresponds to that of water at 140 keV energy (i.e. 0.15/cm). The dense bone had an attenuation coefficient of 0.1/voxel (or 0.25/cm for 140 keV energy). One slice of the map is shown on the left of figure 2. In 2D simulations, this slice was used as the object-specific attenuating medium. For 3D validation, the whole map of 64 slices was employed.

An emission phantom was generated from the attenuation map. First the voxels of the patient bed in the map were set to zero. Then the remaining voxels were segmented into regions of bone, soft tissues, lungs and air. A region of myocardium was synthesized for a cardiac insert. By assigning different activities to the segmented regions (5.0 for the myocardium, 1.0 for the soft tissues, 0.5 for the lung parenchyma and skin, and zero for the bone and air), the emission thorax phantom was then constructed. A slice of the object-specific emission phantom is shown on the right of figure 2. This slice was used for 2D simulations. In order to avoid truncation along the z-axis for 3D simulations when considering the resolution variation, two slices of the emission phantom at both ends were set to zero. The central 60 slices remained.

A system-specific resolution kernel was constructed by measurements of a point source at depths of 1, 5, 10, 15, 20, 25, 30 and 35 cm from the surface of a low-energy, high-

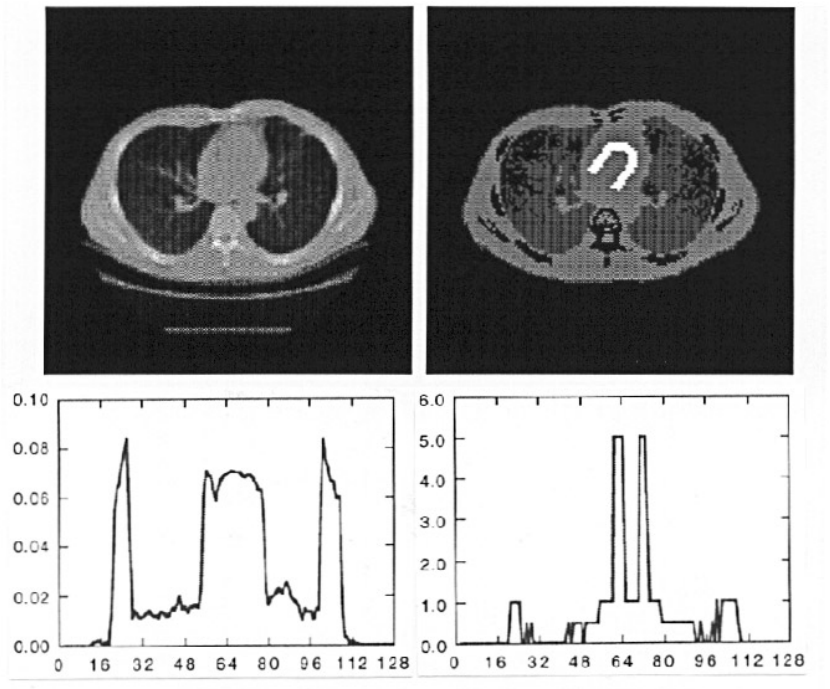

Figure 2. A slice of a patient chest attenuation map (on the left) and an emission phantom (on the right) constructed from a segmentation of the map. The one-pixel-wide profiles were drawn horizontally through the images.

resolution, parallel-hole collimator. The collimator was customarily used for chest SPECT studies in our Nuclear Medicine Division. The point-source images had an array size of 128^2. Each pixel was 4 mm square (the same size as the phantom pixels). The size of the kernel was $128^2 \times 160$, where a total of 160 depths were interpolated with an increment of 4 mm from the measurements. At each depth, the kernel was normalized to 1. In 2D simulations, the central sagittal slice of 128×160 was used, where the normalization was performed for each depth.

Projections were simulated from the emission thorax phantom, the attenuation map, and the resolution kernel by 128 stops evenly spaced on an elliptical orbit. Each projection had 128 bins for 2D studies and 128×64 bins for 3D evaluation. The low-energy, high-resolution, parallel-hole collimator geometry was assumed. In tracing the attenuation factors, the exact model of equation (1) was used. In order to study the effect of the central-ray approximation on the reconstruction accuracy only, the scatter and noise options were turned off in the projection simulations.

In reconstructing the projection data, we first implemented the exact model of equation (1) into the ML-EM (maximum-likelihood and expectation-maximization) algorithm. The reconstructed images were treated as a standard ruler to measure other images reconstructed when the exact model of equation (1) was not used. Then we employed the central-ray approximation model of equation (2) to reconstruct the same projection data. The reconstructions were named as approximated images. The criterion employed to measure the difference of the approximated images from the standard ones is the root-mean-square

error

$$\text{RMSE} = \left(\sum_j (o_j - s_j)^2 \Big/ \sum_j (s_j - \bar{s})^2 \right)^{1/2} \tag{3}$$

where $\{s_j\}$ and $\{o_j\}$ are the phantom and reconstructed source arrays respectively, and $\bar{s}$ is the mean activity of the phantom. For a uniform region, the error is defined as

$$\text{RMSE} = \left(\sum_j (o_j - s)^2 / s^2 \right)^{1/2} \tag{4}$$

where s is the mean activity of the phantom region.

4. Results

The computing time for simulating the 2D projections was approximately 20 min on an HP/730 desktop computer. The reconstruction by the ML-EM algorithm was run up to 1000 iterations to achieve a stable solution. The reconstructed images are shown in figure 3. On the left is the standard image and on the right is the approximated one. The one-pixel-wide profiles were drawn for comparison purpose. Both profiles are almost identical and closely represent the phantom profile on the right of figure 2.

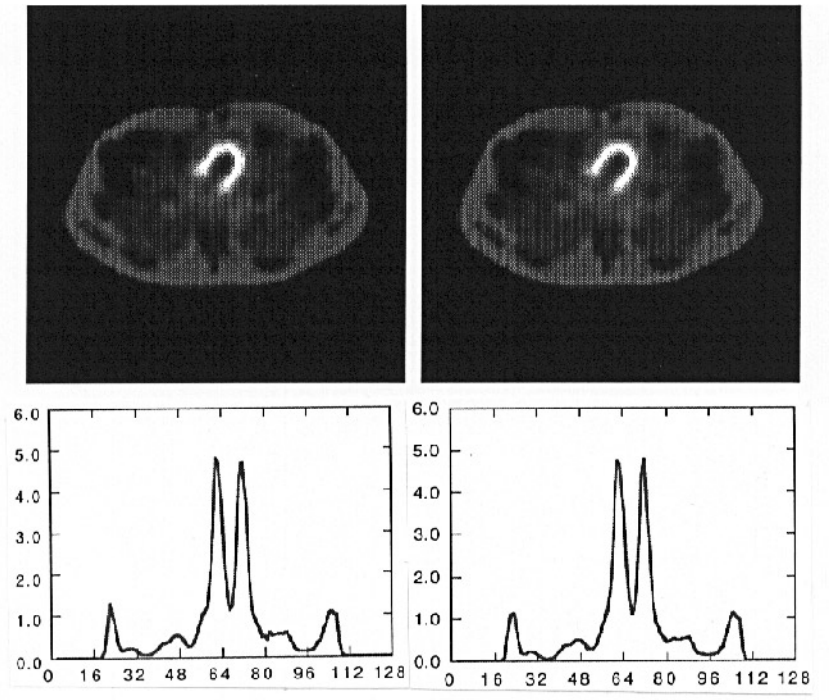

Figure 3. A slice of reconstructions by the exact model (left) and by the approximated model (right). The one-pixel-wide profiles were drawn horizontally at the same position as in figure 2.

The computing time for simulating the 3D projections was more than 15 h by the exact model of equation (1). The simulating time was reduced to less than 8 min by the

approximated model of equation (2). In order to avoid the heavy computing burden by the exact model, we used the approximated model to reconstruct both the simulated 3D projection data. The reconstruction from the projections of approximated model was then treated as the standard image, since the reconstruction algorithm used the same model as the projection simulation did. The reconstruction from the projections of the exact model was assumed as the approximated image, because the reconstruction and the simulation used different models. The central slice of the reconstructed images is similar to that of figure 3. The RMSEs of these two images are listed in table 1. After 1000 iterations, the difference of the RMSEs between the standard and approximated images is 3% for the whole body, 5% for the soft tissues, 2% for the lungs and 1% for the heart.

Table 1. The RMSEs in the selected regions between the standard (left) and the approximated (right) images, as a function of iteration. The values in the second column are computed from the whole phantom, in the third one from the soft tissues, in the fourth one from the lungs and in the fifth one from the heart.

Iteration	Phantom (t,f)	Tissue (t,f)	Lung (t,f)	Heart (t,f)
10	(0.442, 0.444)	(20.21, 20.29)	(10.37, 10.45)	(5.000, 5.020)
50	(0.339, 0.339)	(17.70, 17.75)	(10.81, 10.42)	(3.357, 3.366)
100	(0.304, 0.304)	(16.73, 16.81)	(11.04, 10.55)	(2.755, 2.764)
150	(0.287, 0.288)	(16.08, 16.22)	(11.03, 10.54)	(2.508, 2.516)
200	(0.277, 0.278)	(15.59, 15.79)	(11.00, 10.52)	(2.382, 2.390)
250	(0.270, 0.272)	(15.20, 15.46)	(10.97, 10.50)	(2.308, 2.314)
300	(0.264, 0.267)	(14.89, 15.20)	(10.93, 10.49)	(2.258, 2.264)
400	(0.257, 0.260)	(14.40, 14.78)	(10.88, 10.45)	(2.194, 2.200)
500	(0.251, 0.255)	(14.01, 14.46)	(10.82, 10.42)	(2.152, 2.158)
600	(0.246, 0.251)	(13.70, 14.21)	(10.76, 10.39)	(2.120, 2.128)
700	(0.242, 0.249)	(13.43, 14.00)	(10.70, 10.37)	(2.094, 2.104)
800	(0.239, 0.245)	(13.19, 13.81)	(10.65, 10.36)	(2.072, 2.085)
900	(0.236, 0.243)	(12.98, 13.65)	(10.60, 10.35)	(2.053, 2.070)
1000	(0.233, 0.241)	(12.79, 13.51)	(10.55, 10.34)	(2.036, 2.057)

The mean activity of the myocardium for the approximated image, after 1000 iterations, is different by 0.2% from that of the standard image in 2D simulation, and in the 3D case the error is around 0.4%. The error for the lungs is approximately 0.4% in the 2D case, and 0.7% in 3D simulation. The error is a negligible bias for quantitative heart and lung SPECT studies, both of which are the most important studies in chest SPECT imaging.

When the resolution variation was neglected in the ML-EM reconstruction of the projections of the exact model equation (1), the RMSEs increased to 48% for the whole body, 34% for the soft tissues, 17% for the lungs and 72% for the heart, after 1000 iterations. The reconstruction did not converge to a stable solution. It seemed to diverge for further iterations. The subtracted image of the reconstruction from the phantom is significantly different from those two subtractions which compensated for the resolution variation and were very similar. The voxel values for the subtraction of the reconstruction (without resolution compensation) from the standard image vary in the range $(-1.7, +2.4)$, while the subtraction of the approximated image (with resolution compensation) from the standard one has voxel values in the range $(-0.4, +0.4)$. Compensation for the resolution variation is necessary for quantitative SPECT imaging. The central-ray approximation offers the opportunity to achieve the compensation in an efficient and accurate manner.

The reconstruction time could be more than a day per iteration for the exact model and was approximately 15 min for the approximated model. The reduction of computing time

is dramatic. The program was coded by Fortran 77. Further reduction of computing time can be achieved by optimizing the code.

5. Conclusion

A validation study on the central-ray approximation for quantitative SPECT reconstruction was performed using accurately measured object-specific attenuation map and system-specific resolution kernel. The approximation reduced the computing time dramatically with a negligible loss of reconstruction accuracy. The approximation is necessary for analytical inversion of the SPECT projection equation (Liang *et al* 1994) and is clinically useful for iterative reconstruction (Ye *et al* 1994).

Acknowledgments

This work was supported by grant #HL51466, awarded by the National Heart, Lung, and Blood Institute; grant #NS33853, awarded by the National Institute of Neurological Disorders and Stroke; and Established Investigator Award from the American Heart Association; and in part by an Award from ADAC Company and a Seed grant from the Society of Thoracic Radiology.

References

Appledorn C R 1989 An analytical solution to the nonstationary reconstruction problem in SPECT *Proc. IPMI* **11** 69–80

Glick S J, Penney B C, King M A and Byrne C L 1993 Noniterative compensation for the distance-dependent detector response and photon attenuation in SPECT imaging *Conf. Record IEEE NSS-MIC* **2** 1172–4

Jaszczak R J 1988 Tomographic radiopharmaceutical imaging *Proc. IEEE* **76** 1079–94

Liang Z 1992 Compensation for attenuation, scatter, and detector response in SPECT reconstruction via iterative FBP methods *Med. Phys.* **40** 1097–106

Liang Z, Jaszczak R J, Floyd C E, Greer K L and Coleman R E 1988 Bayesian reconstruction of SPECT in parallel, fan, and cone beam geometries *J. Nucl. Med.* **29** 871

——1989 Reprojection and backprojection in SPECT image reconstruction *Proc. IEEE Southeast'89* **1** 919–26

Liang Z, Ye J and Harrington D P 1994 An analytical approach to quantitative reconstruction of nonuniformly attenuated brain SPECT *Phys. Med. Biol.* **39** 2023–41

Riauka T A and Gortel Z W 1994 Photon propagation and detection in SPECT—an analytical approach *Med. Phys.* **21** 1311–21

van Elmbt L and Walrand S 1993 Simultaneous correction of attenuation and distance-dependent resolution in SPECT: an analytical approach *Phys. Med. Biol.* **38** 1207–17

Ye J, Liang Z and Harrington D P 1994 Quantitative reconstruction for myocardial perfusion SPECT: an efficient approach by depth-dependent deconvolution and matrix rotation *Phys. Med. Biol.* **39** 1263–79

Zeng G L and Gullberg G T 1992 Frequency domain implementation of the 3D geometric point source response correction in SPECT imaging *IEEE Trans. Nucl. Sci.* **38** 693–702